# Plasma Electrolytic Nitrocarburizing of SAE 1045: Electro-chemical Slurry Erosion Wear Analysis

*Leandro Câmara Noronha[a]** ⓘ, *Victor Velho de Castro[a], Roberto Moreira Schroeder[a],*

*Leonardo Mussulini[a], Leonardo Moreira dos Santos[b],*

*Antonio Marcos Helgueira de Andrade[c], Célia de Fraga Malfatti[a]* ⓘ

[a]*Universidade Federal do Rio Grande do Sul (UFRGS), Laboratório de Pesquisa em Corrosão (LAPEC), Porto Alegre, RS, Brasil.*
[b]*Pontifícia Universidade Católica do Rio Grande do Sul (PUCRS), Escola Politécnica, Laboratório de Química, Porto Alegre, RS, Brasil.*
[c]*Universidade Federal do Rio Grande do Sul (UFRGS), Instituto de Física, Porto Alegre, RS, Brasil.*

Nitrocarburized coating by plasma electrolytic saturation, PEN/C coatings, have been proposed to increase the corrosion and wear resistance of steel by using a process of low-temperature hydrostatic plasma. The objective of this work is to analyse the wear and corrosion resistance of PEN/C coatings on SAE 1045 steel, using the electrochemical slurry erosion wear test (ESEWT). This test allows the evaluation of the simultaneous effect of erosion wear and electrochemical behaviour on this coating. Thus, it was possible to evaluate the erosive and corrosive effect and the synergy of these phenomena on the PEN/C coated SAE 1045 mass loss rates. ESEWT tests were performed at different times and under different electrochemical conditions: under cathodic protection and open circuit potential (OCP). The PEN/C coating increased the corrosion resistance of SAE 1045. Synergy between the erosive wear and corrosion was the main factor in the mass loss rates of both analysed systems. The synergistic mechanism of the substrate occurred by removing the corrosion product and by activating the surface generated by the erosive process of the particles. The synergistic mechanism of the PEN/C coating occurred with the removal of inherent surface irregularities through the erosive process, combined with localized corrosion.

**Keywords:** *slurry erosion wear, corrosion, plasma electrolytic saturation, steel.*

## 1. Introduction

Nitrocarburized coating by plasma electrolytic saturation (PEN/C, also called plasma electrolyte saturation (PES)[1] or electrolytic-plasma saturation (EPS)[2] is an atmospheric pressure plasma process which forms a nanostructural coating. The main advantages of plasma electrolytic treatments are the high processing speed and low cost[3]. The principle of the technique is based on traditional chemical heat treatment. The sample acts as an electrode connected to a power source and serves as the cathode, submerged in the electrolyte. Once a stable hydrogen film is formed on the sample by applying high voltage, an electrical discharge, including electron and ion avalanches, occurs through the hydrogen. Then, the sample is heated drastically due to the generation of resistance heat in a short time and the local temperature in the discharge area can reach a very high value, which can be above the austenitization temperature[4]. The plasma envelope is formed around the surface, which induces the bombardment of particles and free radicals on the surface. Thus, diffusion occurs on the surface of the sample[5].

As a carbonitriding process carried out by different techniques, this surface modification process is carried out by diffusion. Thus, N and C ions diffuse between the surface layers of the metal, forming a diffusion layer. As the process evolves, N and C saturation occurs in this region, leading to the formation of a layer of nitrides and carbides on the surface, normally called a layer of compounds[6].

As expected, the composition of the gaseous envelope that forms around the substrate is dependent on the chemical composition of the electrolyte. In aqueous solutions water vapor is the main component in case an organic component is present in the electrolyte, for example, for nitrocarburization the following reactions can occur[2]. According to Padervan et al.[7], PEN is a cathodic atmospheric plasma process that has shown promising deposition of metallic coatings that exhibit significant adhesion to the substrate, as well as high deposition rates.

Thus, this technique has been applied in medium carbon steels, aiming to improve the wear resistance and corrosion resistance of these materials[3,8,9]. In the study by Tambovskiy et al.[8], the possibility of using an aqueous non-toxic electrolyte of ammonium nitrate and glycerin for cathode plasma electrolytic nitrocarburizing of low carbon steels was analyzed. The surface morphology and roughness, element and phase compositions, and microhardness of the modified layer were investigated. The presence of a dense oxide layer, low surface roughness and high hardness of the diffusion layer favor a reduction in the friction coefficient by 1.3 times, wear by 1.8 times and the corrosion current density by 1,4 times.

*e-mail: leandro.noronha@ufrgs.br

The relationship between surface chemistry and corrosion resistance of electrochemically nitrided AISI 304 stainless steel samples was investigated by Rocha et al.[10]. Nitriding treatment was carried out in 0.1 M HNO3 and 0.1 M HNO3 + 0.5 M KNO3 at room temperature. The corrosion behaviour of the nitrided samples was evaluated by potentiodynamic polarization. The results showed that the nitrided layers consisted of a mixture of chromium nitrides, chromium oxides, iron oxides/oxyhydroxides and nickel oxide. The best corrosion resistance was obtained by electrochemical nitriding in the 0.1 M HNO3 + 0.5 M KNO3 solution as it presented higher concentrations of nitrogen atoms in the layer.

Erosion due to abrasive slurries occurs in many engineering applications, in many cases of ductile materials. Normally, less attention is given to the wear under normal impact conditions and this phenomenon is poorly understood[11]. Erosion wear is recognized as a problem in slurry handling and transportation equipment such as centrifugal pumps. It is widely used in numerous industries[12]. The erosion–corrosion process involves two different mechanisms, and the synergy between them, which leads to the degradation of materials. The two mechanisms can be said to be mechanical erosion and chemical corrosion[13,14].

Many works have studied the slurry erosion wear and corrosive phenomena in coated turbine steel[15-17]. Mud erosion tests of SUS-304 stainless steel was performed using alumina sand and water flows. It was shown that the erosion rate was reduced over the test time and the erosion rate increased with increasing impact velocity. Two different erosion regimes occurred: plastic deformation and plugging/cutting[18]. Javaheri et al.[19] studied the grain refinement of a medium-carbon used as a material for slurry transport piping. It was demonstrated that the grain size of austenite had no significant effect on the final microstructure and hardness value. However, variations in the martensite block size formed influenced the hardening behaviour and, consequently, the wear mechanism of the samples during the tests.

The phenomenon of erosion wear in different materials (aluminium alloy (AA6063), copper, brass, ductile steel, AISI 304L stainless steel, AISI 316L stainless steel and turbine blade steel) were studied in a slurry tester[20]. Three erodents were used: quartz, alumina and silicon carbide. The roughness of the worn surfaces indicated that the penetration of solid particles into the surface of the target material is a function of the hardness range of the erodent and the target material. In addition, it was proposed that the erosive wear of ductile materials appears to be a function of the relationship between the erodent hardness and target material hardness and has a strong dependence on velocity (the wear rate increases with increasing velocity) and particle size (decreases the wear rate with increasing size).

Nitrocarburized layers, formed by the PEN/C process, which have not yet been studied in relation to the participation of each degrading factor, wear, corrosion and synergy, appear as an alternative to mitigate the erosive and corrosive effect of low carbon steel samples. Therefore, the electrochemical slurry erosion wear test (ESEWT) technique[15,21], developed by our research group, is perfectly applicable to the study of the participation of each variable mentioned above, as long as it is supported by the ASTM G119 standard[22].

During the ESEWT test, only hydrodynamic stresses are applied to the surface, reaching values close to 42 kPa at tangential velocities of 8.2 m.s[-1 21]. Other authors report that only substantially higher stresses are capable of altering erosive wear mechanisms[23]. This study demonstrated that higher rotational speeds during the test can increase the rate of erosive wear. Furthermore, rotational speeds favour the supply of oxygen to the surface and generally increase the corrosion rate of metallic materials.

The objective of this work is to analyse the resistance to wear, and corrosion of the PEN/C coating applied to SAE 1045 steel samples, using the electrochemical slurry erosion wear test (ESEWT), in the presence of abrasive particles suspended in a solution of water and 0.5% (wt.%) of NaCl. From the ESEWT it is possible to evaluate the erosive wear, the corrosion, and the synergy of these phenomena on the PEN/C coated SAE 1045 mass loss rate.

## 2. Materials and Methods

To obtain a PEN/C coating, SAE 1045 steel discs were used. The samples were machined to dimensions of 15 mm in diameter and 4.5 mm in thickness. The area of the exposed sample (in contact with the electrolyte) was 113 mm$^2$. The chemical composition of the steels used was analysed by the Bruker Q2 ION optical emission spectrometer. The samples were sanded with silicon carbide sandpaper with a grain size of #120 to #1000. After sanding, cleaning was performed with water and neutral detergent, followed by cleaning with acetone, and the samples were subsequently dried with forced air.

The electrolyte and initial parameters to obtain the PEN/C coatings were based on the article by Noori and Dehghanian[5]. The electrolyte used (20 L) after the initial adjustments was composed of 6 gL$^{-1}$ of $C_3H_8O_3$ (glycerol) and 24 gL$^{-1}$ of $NaNO_2$ (sodium nitrite). The electrolyte temperature was maintained above 80 °C. As a counter electrode, a stainless steel screen was used. The PEN/C process was conducted by using an AC source with a frequency of 1500 Hz and duty cycle of 40 %. The maximum values of positive and negative voltage were 450 V to 0 V (cathodic potential). The process lasted 20 min. Before obtaining the PEN/C coatings, the SAE 1045 steel samples were immersed for 20 s, to carry out chemical pickling, in a solution of deionized water and 0.1 M HCl. After this procedure, the samples were immersed for 5 min in acetone. The cleaning and chemical stripping procedure followed the recommendation of other authors[5]. The phases formed in the coating were determined by a Bruker model D8 ADVANCE diffractometer with Cu-Ka incident radiation (l = 0.15418 nm), and measurements were conducted with Bragg-Brentano θ - 2θ geometry (step size = 0.020; power = 40 kV – 40 mA; and time per step = 384 s). The hardness profile of the cross-section of the coated and uncoated samples was performed using the Buehler microdurometer, model 1600. The applied load was 50 g. To measure the gradient, we moved 3 μm in the depth direction and 50 μm lateral displacement within the layer itself, allowing for the correct distance between indentations.

The electrochemical slurry erosion wear test (ESEWT) was carried out in an erosive test equipment in an aqueous medium, where it is possible to carry out electrochemical tests simultaneously, which was developed in the laboratory

itself and has a patent deposition n° BR 10 2019 015849 2 and applied in previous studies[15,21].

The linear velocity (VL) used was 8.2 m.s$^{-1}$. As an aqueous medium (constant volume of 6 L), a suspension of silica particles (erodent) in the proportion of 2.5% (wt.%) and 0.5% (wt.%) of NaCl was used as electrolyte. The presence of NaCl in the electrolyte used aimed to increase the aggressiveness of the solution in corrosive terms. It can also be remembered that all natural waters contain NaCl.

The electrolyte temperature was controlled during the ESEWT test and no significant temperature variations were detected. Therefore, this study was carried out at a constant temperature (21 °C).

The suspension/electrolyte had a neutral pH (between 6.5 and 7.5). The granulometric distribution of the silica particles was determined using a Cilas 1180 laser diffractometer.

To determine the effect of erosion on the corrosion resistance of the coatings and substrate, polarization curves were performed immediately after immersion (0 h), and after 1 h, 2 h, 4 h and 8 h of testing, with cathodic protection of -1000 mV$_{sce}$. Polarization curves were performed using a three-electrode cell, with the sample being the working electrode, against graphite electrode and saturated calomel as reference electrode. The curves were made from cathodic potentials, with values of -1000 mV$_{sce}$ to 0 mV$_{sce}$. The sweep speed was 1 mV.s$^{-1}$. Tests were also carried out at open circuit potential, during the same test times. The erosive, corrosive and synergistic effects that occurred during the ESEWT on the samples were studied following the recommendations of ASTM G 119[22]. For the electrochemical tests, to obtain the I$_{corr}$ and the corrosion rate (CR) using the Tafel method, potentials of 20 mV above the E$_{corr}$ of the different samples were applied, reading the generated current, after time for stabilization, in tests with erosion, following the recommendations of the ASTM G102-89 standard[24].

Samples of the average surface roughness (Ra) (arithmetic mean of the absolute values of the spacing ordinates, of the roughness profile points in relation to the midline, within the measurement path) and average surface roughness of the five highest partial values (Rz) were analysed in coated and uncoated steel samples. Analyses were performed before and after the ESEWT tests. A Mitutoyo SJ-410 rugosimeter was used. The recommendations of the ISO 4287:1997 standard was followed[25].

The weight loss of the samples was determined by weighing them on a Shimadzu precision scale, model AY220, before and after the erosive/electrochemical tests. The surface morphology of the samples before and after the tests was analysed with the field emission scanning electron microscope (FESEM) Inspect F50 and a Zeiss optical microscope model Axio Lab.A1. For image analysis, ZEN 2.6 software (blue edition) was used.

## 3. Results

### 3.1. Characterization

Table 1 presents the characterization of the steel samples used in this study. The chemical composition obtained was that expected for SAE 1045 steel. The percentages of the measured elements in weight percent are presented below: Fe = balanced; C = 0.47%, Si = 0.15%, Mn = 0.02%, P = 0.02%.

The hardness of the samples was approximately 210 HV, which is compatible with the pearlitic and ferritic microstructure of these samples. As expected, XRD analysis (Figure 1D) detected only the α-Fe phase (JCPDS NO: 00-052-0512). Due to surface polishing, the average roughness Ra and Rz of the samples were approximately 0.04 μm and 0.26 μm, respectively.

Figure 1A shows the surface morphology of the coating formed. In the cathodic plasma electrolysis process, a continuous vapor envelope around the part is ruptured at a critical voltage, resulting in the generation of plasma discharge in the region close to the cathode[26]. The pores observed (diameter varied between 8.0 μm and 22.5 μm, with an average diameter of 16.5 ± 5.5 microns) on the surface of the sample are the plasma discharge channels remaining after the PEN/C process[27]. Other authors propose that the change in the morphology of the steel surface during PEN/C is associated with the occurrence of oxidation and surface erosion at high temperature, characteristic of cathode electrodes in aqueous electrolytes. Under the action of electrical discharges, the layer erodes, which leads to the formation of craters[8].

In addition to the discharge channels, it is also noticed that the surface topography of the samples was uneven, generating a higher roughness than the substrate after surface preparation, as shown in Table 1. The thickness of the layer formed, measured in the cross-section image of the coated samples (Figure 1B), was approximately 20.50 μm ± 4.5 μm thick. The coating obtained cannot be precisely controlled, but the operational parameters influence the regularity and thickness. In the work of Hua et al.[28], for example, the concentration of ammonium in the electrolyte influenced the thickness and properties of the layer obtained.

No regions with delamination were detected in the layer formed with the parameters used. However, it is known from the literature[29] that the choice of parameters different from those used in this work can generate delamination or poor adhesion, for example, the application of anodic potentials in PEN/C instead of cathodic potentials (applied in this work).

XRD analysis detected the formation of iron nitrides $\varepsilon - Fe_{2-3}N$ (JCPDS NO: 01-083-0878), $\gamma' - Fe_4N$ (JCPDS NO: 01-083-0879) and $Fe_3C$ (JCPDS NO: 03-065-2415). Also detected was $Fe(Fe(C_9N)_6)_3$[5]. Therefore, the presence of these phases suggests that the concentration of carbon and nitrogen in the surface layers was so high that it had exceeded the solubility limits of carbon and nitrogen in iron, forming this protective coating on the samples surfaces[30]. It is known that the formation of $\varepsilon - Fe_{2-3}N$ makes it possible to increase the hardness of the coating formed and increase the wear resistance[31,32].

Table 1. Chemical composition, hardness and roughness of the SAE 1045 steel samples. Values in parentheses represent the standard deviation.

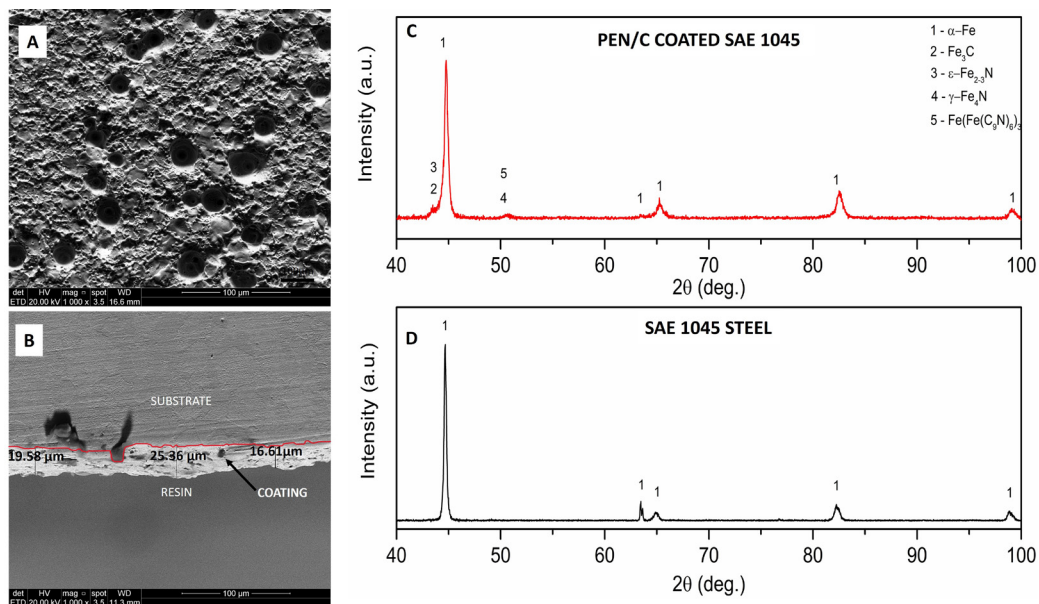| Samples | Hardness (HV) | Ra (μm) | Rz (μm) |
|---|---|---|---|
| SAE 1045 | 210 | 0.04 | 0.26 |
| | (30) | (0.02) | (0.05) |
| PEN/C COATED SAE 1045 | 1040 | 1.05 | 8.03 |
| | | (0.12) | (1.15) |

**Figure 1.** Characterization of the PEN/C coated SAE 1045. A: SEM of the coating surface of PEN/C coated SAE 1045 ; B: Cross-section and layer thickness measurement; C: XRD of PEN/C coated SAE 1045; D: XRD of the SAE 1045 steel substrate.
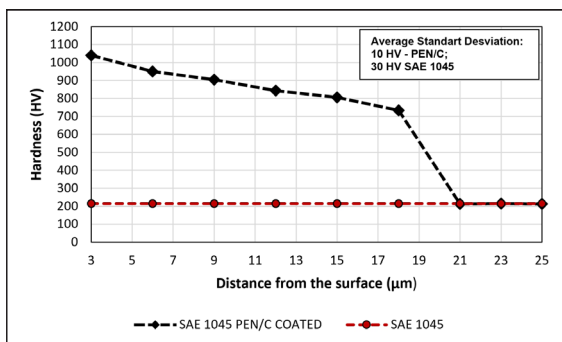


**Figure 2.** Hardness profile of the studied samples.

It should be noted that in other works involving nitrocarburizing, carbon could be associated with the nitrides formed, generating the $\varepsilon$-$Fe_{2-3}$(C,N) and $\gamma$'-$Fe_4$(C,N) phases[33,34]. According to Li et al.[35] increasing carbon content increases the formation of the $\varepsilon$-$Fe_{2-3}$ (C, N) phase in the composite layer according to the Fe–N–C ternary phase diagram. However, it is difficult to determine whether the phases in the layer are nitrides or carbonitrides, as the lattice spacing in iron nitrides or carbonitrides is almost the same.

Figure 2 shows the hardness profile of the cross-section of the PEN/C coated SAE 1045 samples and the uncoated sample. It is noticed that the SAE 1045 steel has a homogeneous microhardness, presenting values close to 200 HV. However, as expected, the surface hardness of the samples with the nitrocarburized layer has a substantially higher microhardness than the substrate. At the first measurement point (3 µm from the surface), the coating showed a maximum hardness of approximately 1040 HV, which is associated with the

phases: $\varepsilon - Fe_{2-3}N$, $\gamma' - Fe_4N$ and $Fe(Fe(C_9N)_6)_3$ detected in the XRD analysis (Figure 1C)[31,32]. As shown in Figure 1B, the coating has a thickness ranging from 16 µm to 25 µm. As can be seen, this layer showed a variation in thickness. Apparently, this thickness variation is due to the PEN/C process, according to Belkin, et. all[3]. Thus, the microhardness of the sample, up to approximately 18 µm from the surface, showed a slight downward trend to values close to 730 HV. At greater distances from the surface in cross-section, a rapid decrease in hardness occurred, with values similar to those of the substrate, indicating the end of the coating. Therefore, a diffusion layer was not detected in the SAE 1045 samples with PEN/C coating at thicknesses less than the nitrocarburized layer. Due to the hardness scale shown in Figure 2, it was not possible to visualize the results dispersion bar for the microhardness measurement, which were close to ± 10 HV in the PEN/C coated SAE 1045 sample and ±30 HV in the SAE 1045 sample.

Figure 3 presents the characteristics of the eroded particles used in this study. Figure 3A presents the image of the geometry of the eroded particles. It is noticed that there is a mixture of particles with angular geometry, which favour the loss of mass by the erosion process, and particles with more spherical geometries, which reduce the loss of mass[36]. According to Clark and Llewellyn[37], silica particles are classified as fairly rounded and are responsible for severe damage caused by erosive wear in industry. However, the XRD analysis (Figure 3B) predominantly detected $SiO_2$ - quartz (JCPDS NO: 01-087-2096 and 00-003-0427), which may be more angular[37], and particles with these characteristics were also found. It is known that the hardness of this type of silica is approximately 750 HV[37]. In addition, it is worth noting the fact that no contaminants were detected, which could alter the results of wear and corrosion.
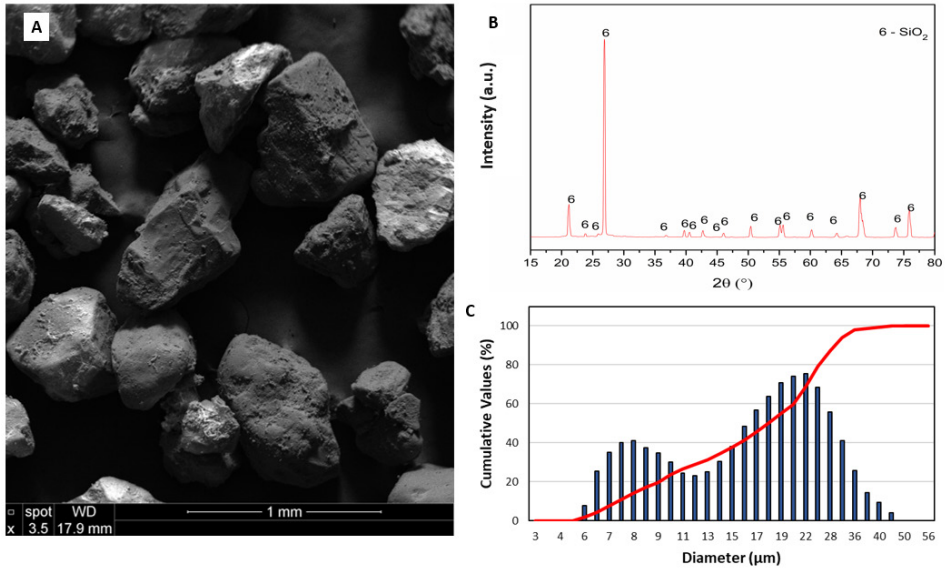
**Figure 3.** Characterization of the erodent used. A: SEM of erodent particles - 60x; B: XRD of erodent particles; C: Particle size distribution of eroded particles.

Figure 3C shows the granulometric distribution of the erodent used in the tests. The particles showed a bimodal distribution, that is, they did not show a Gaussian distribution. However, it is noted that the particles had dimensions smaller than 50 μm. In the work of Lynn et al.[38], it was demonstrated that, for these suspensions with particle sizes greater than about 100 μm, the erosion rate is proportional to the kinetic energy dissipated by the particles during the impact, but for particle sizes smaller than 100 μm, as in the case of the silica used in this study, other metal removal mechanisms become increasingly significant. In another study[39], the addition of particles sizes less than 75 μm reduced slurry erosion wear. According to these authors, this phenomenon can be attributed to the partial increase in viscosity of the carrier fluid, partial decrease in turbulence and partial decrease in impact velocity, due to particle-particle collision and the formation of a thin layer of particles on the eroded surface. The wear reduction, however, does not vary with the impact angle and particle size distribution. Furthermore, the kinetic energy of particles smaller than 100 μm quickly becomes less and the impact ceases completely. Thus, particles that fail to recover from the target's surface after impact could accumulate on the target's surface. When swept away by the fluid flow, these accumulated particles could erode the target surface[40].

## 3.2. Electrochemical slurry erosion wear test

### 3.2.1. Polarization curves

The electrochemical slurry erosion wear test (ESEWT) was performed on samples containing the nitrocarburided layer and samples without surface treatment. The electrochemical results of the tests at time zero (started immediately after immersion in the suspension/electrolyte) are shown in Figure 4A. Table 2 shows, among other results, the $E_{corr}$ and $I_{corr}$ of the polarization curves performed at time zero through the ESEWT test.

The SAE 1045 steel presented a more active $E_{corr}$ (- 423 mV$_{sce}$) and a higher $I_{corr}$ (2.31 x $10^{-5}$ A.cm$^2$) compared to PEN/C coated SAE 1045 (Figure 3A and Table 2), which presented an $E_{corr}$ in - 375 mV$_{sce}$ and $I_{corr}$ of 0.61 x $10^{-5}$ A.cm$^{-2}$, resulting in a corrosion rate of 0.35 mm.year$^{-1}$ and 0.13 mm.year$^{-1}$, respectively. This increase in the corrosion resistance of medium carbon steels is due to the formation of layers with protective characteristics, such as the nitrocarburized layer[41]. Studies show that the protective effects provided by a combination of the oxide layer and the nitrocarburized zone can significantly increase the corrosion resistance of low carbon steels[42].

**Table 2.** $E_{corr}$ and $I_{corr}$ values of the polarization curves performed immediately after immersion in the suspension/electrolyte.

| Material | Parameter | Time zero |
|---|---|---|
| SAE 1045 | $E_{corr}$ (mV$_{sce}$) | - 423 |
| | $I_{corr}$ [$10^{-5}$] (A.cm$^{-2}$) | 2.31 |
| | CR (mm.y$^{-1}$) | 0.35 |
| PEN/C COATED SAE 1045 | $E_{corr}$ (mV$_{sce}$) | - 375 |
| | $I_{corr}$ [$10^{-5}$] (A.cm$^{-2}$) | 0.61 |
| | CR (mm.y$^{-1}$) | 0.13 |

The small difference observed between steel with PEN/C and without coating must be associated with the existence of discharge channels (pores) that are inherent to the layer formation process. It should be noted that this difference in corrosion resistance, generated by the nitrided layer, can be reduced over time, since the polarization curve is carried out in relatively short times. With longer immersion times, it can facilitate the permeation of electrolyte in the observed discharge channels, increasing the aggressiveness of the electrolyte occluded in pores, and consequently, increasing the corrosion rate. It is noted that the formation of corrosion products occurred only inside and around the pores and not in the region between the discharge channels, as shown in Figure 4B and Figure 4C. This corrosion product, in fact, must be from the substrate, due to the characteristic coloring of hematite[43].

It is known that coatings formed by PEN/C coated SAE 1045 may have reduced corrosion resistance due to the formation of pores, inherent to the PEN/C process[44].

In the optical microscopy images performed on these samples (Figure 3B and Figure 3C), the formation of corrosion products is observed, preferably in the region of the pores identified in Figure 1A. Previous studies have also demonstrated that the increase in porosity, even in coatings with a thickness greater than that of this study, can contribute to the decrease in the corrosion resistance of samples with this type of coating[44]. Thus, the negative effect that the discharge channels (pores) had on the corrosion resistance of these coatings is confirmed. It can be inferred that the presented porosity has a great role in the corrosive process. Due to the presence of this localized corrosion inside the pores, passivity on the steel (Figure 4B and Figure 4C) in the PEN/C layer is also not observed since the current densities are between $10^{-4}$ and $10^{-3}$ A.cm$^{-2}$. In this sense, it can be assumed that the use of a sealant would greatly contribute to increasing even more the corrosion resistance of the nitrocarburized layer, which already presents high resistance to wear, as will be discussed below in item 3.2.2.
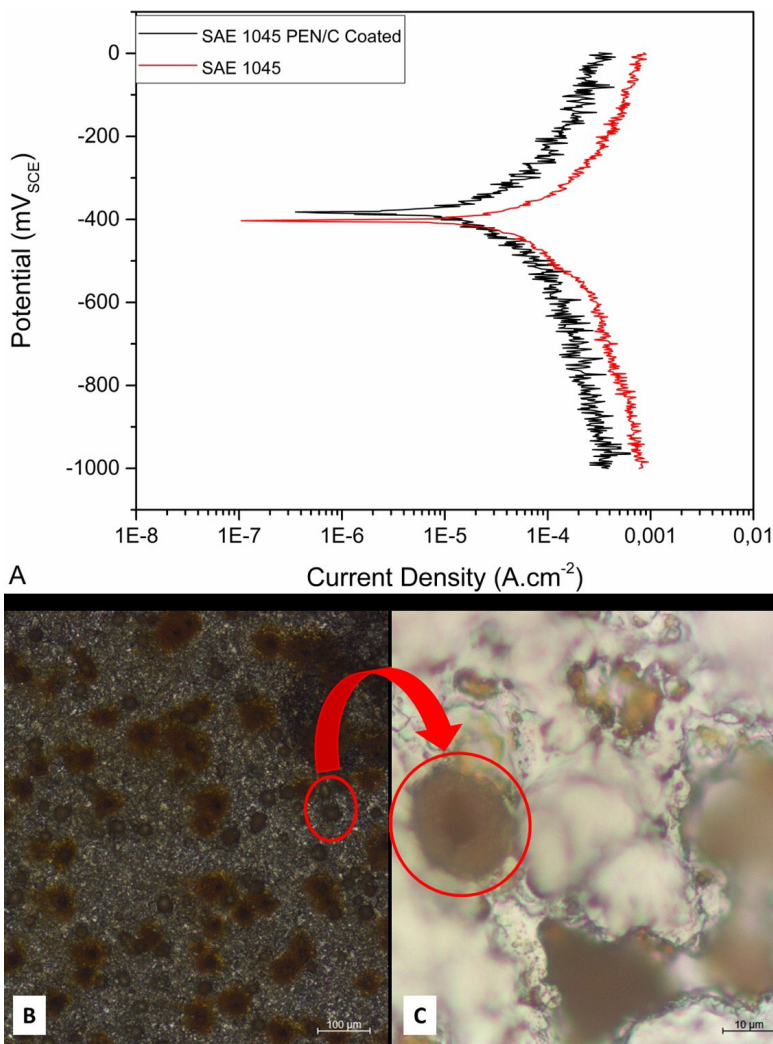


**Figure 4.** Corrosion tests for time zero. A: Polarization curves - erodent 2.5%wt, 1 mv/s, NaCl 0.5%wt.; B: Optical microscopy of PEN/C coated SAE 1045 after the test of 4 hours – 100 x; C: Optical microscopy of PEN/C coated SAE 1045 before the test of 4 hours - 1000x.

## 3.2.2. Weight loss

Figure 5 shows the mass loss and mass loss rate (Figure 6) of the coated and uncoated samples at different ESEWT test times. The tests were performed with cathodic protection and at open circuit potential (OCP), at different test times. Figure 5A presents the results for the SAE 1045 steel samples without coating in the cathodic potential: only the erosive wear was acting in these samples. Note the gradual increase in mass loss as the test time increased. This increase followed a logarithmic trend curve. This occurred due to the surface hardening that this material suffered over time, reducing wear. Thus, after 8 h of testing, the uncoated sample lost approximately 0.7 mg of material. In another study, Wang and Wang[45] analysed the performance of a medium manganese steel in resistance to erosive wear in an aqueous medium. At different angles of eroding incidence and erosion speeds, the resistance to erosion wear of the medium steel manganese was superior to martensitic steel. The formation of wear-hardened layer, caused by the hardening effect, was the fundamental reason for the improvement of wear resistance.

In the case of the OCP tests, the mass loss was significantly higher than the cathodic protection test. This is due to the combined effect of erosive wear and corrosive wear, leading to a mass loss of 9.23 mg after 8 h of testing, following an approximately linear trend curve. In the case of PEN/C coated SAE 1045 samples (Figure 5B), as expected, there was also an increase in mass loss when the ESEWT test time was increased, although substantially less (approximately 3.5 x less than the SAE 1045 steel in the OCP after 8 h of testing). The trend curves, for the PEN/C coated SAE 1045 samples, had an approximately linear behaviour in the tests with cathodic protection and in the OCP. In these samples, there was no significant hardening, due to the high hardness of the coating, leading to a linear behaviour.

The mass loss rates of both systems studied (Figure 6), however, tended to decrease as the test time increased. In the case of uncoated samples, this decrease in the rate is possibly related to the surface hardening created by the plastic deformation of the surface and the consequent increase in surface roughness. Thus, in tests with cathodic protection (Figure 6A), there was a decrease of approximately 2.7 x in the wear rate per year. This trend also occurred in the OCP tests (Figure 6B), although at higher mass loss rates. In the case of nitrocarburized samples (Figure 6C and Figure 6D), the mass loss rate also showed a tendency to decrease over time. However, unlike the untreated samples, the decrease in the rate is due to the removal of surface imperfections from the coating, as shown in Figure 7, consequently leading to a decrease in surface roughness (Figure 8). Thus, these phenomena led to a decrease in wear rates over time, with an approximately logarithmic trend. It should be noted that the trend curves are valid for the test times performed (up to 8 h). However, an extrapolation for longer times, based on the mechanisms presented for the reduction, suggests that the wear rate will stabilize.

Figure 7 shows the SEM analyses of the surface of the samples after the ESEWT tests, after the polarization curves shown in Figure 4A, of the samples without treatment and with PEN/C coating. According to Heinz and Gahr[46], the erosion process of the studied systems can be classified as flush-erosion and erosion-corrosion. In the case of slurry erosion wear, it is known that it is a complex phenomenon and occurs through the interaction of many parameters, such as the characteristics of the erosive particles, properties of the eroded material, operating conditions and the different erosion mechanisms. It is generally assumed that erosion is generated by two main mechanisms, referred to as microcutting and plastic deformation[47]. It is dependent on the impact angle of the particles and the tenacity of the target material (brittle or ductile materials)[48].
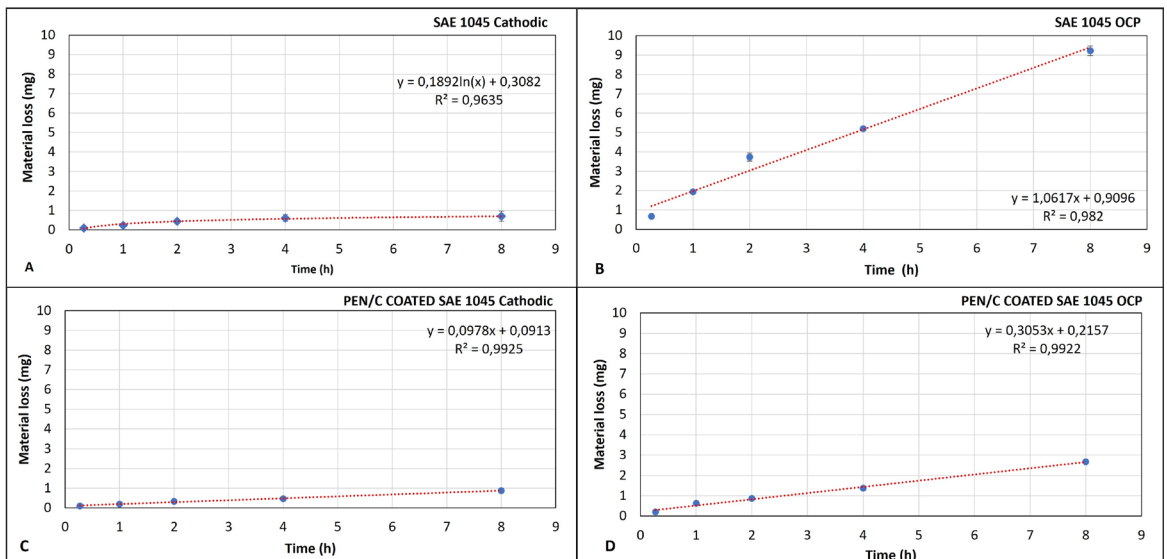


**Figure 5.** Samples mass loss of over-exposure time. A: SAE 1045 (cathodic protection); B: SAE 1045 (OCP); C: PEN/C coated SAE 1045 (cathodic protection). D: PEN/C coated SAE 1045 (OCP).

Thus, this type of wear can be analysed in terms of separating the contributions of deformation wear and cutting wear, each associated with a specific energy value, to remove a unit volume of material[49].

The surfaces of the SAE 1045 steel samples in the 1 h and 2 h tests showed surface defects from a combination of plastic deformation and erosive wear. Therefore, the formation of deformed zones and craters caused by the wear sub-mechanisms of microplugging and microcutting is observed, which occur at angles of incidence close to or less than 40 ° (the angle of incidence of the equipment is 45 °).

The severity of these defects was greater in the 4 h trial. In the case of the 4 h and 8 h tests, for the substrate, the increase in corrosivity with increasing time, commented on below in item 3.2.4, favoured the oxides formed due to the anodic reactions during the polarization curve. Possibly, the rate of formation of these oxides was greater than the rate of material removal by erosive wear. Therefore, the formation of surface cracking was observed, resulting from the impact of particles on fragile materials such as Fe oxides[46]. Thus, the formation of oxides and surface defects led to an increase in the roughness of these samples, as shown in Figure 8.
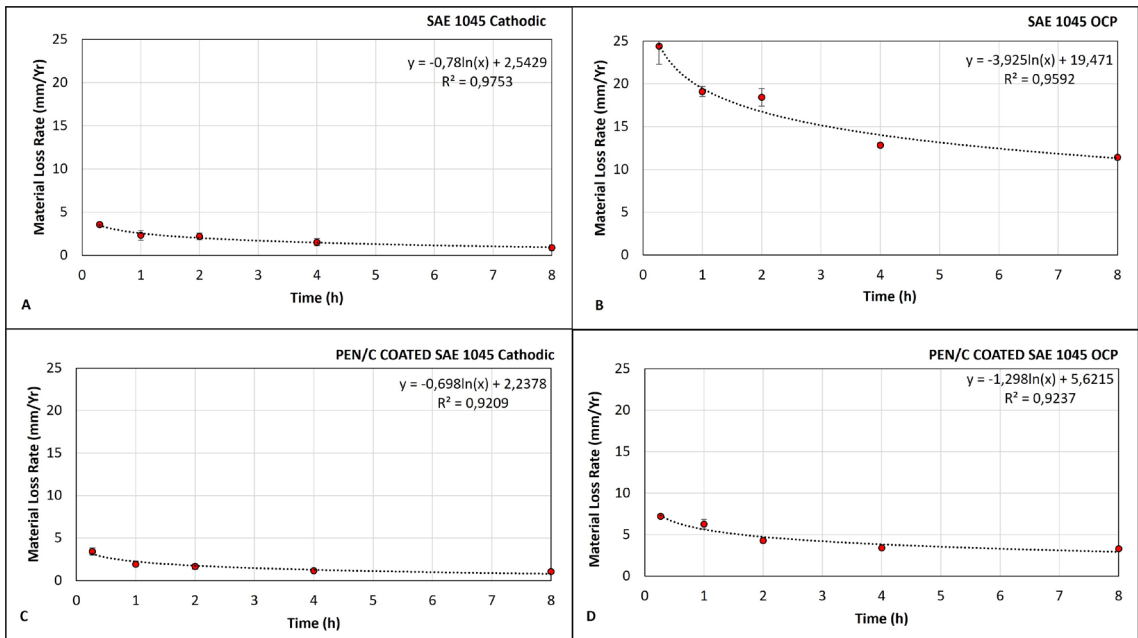


**Figure 6.** Samples mass loss rate over exposure time. A: SAE 1045 (cathodic protection); B: SAE 1045 (OCP); C: PEN/C coated SAE 1045 (cathodic protection). D: PEN/C coated SAE 1045 (OCP).
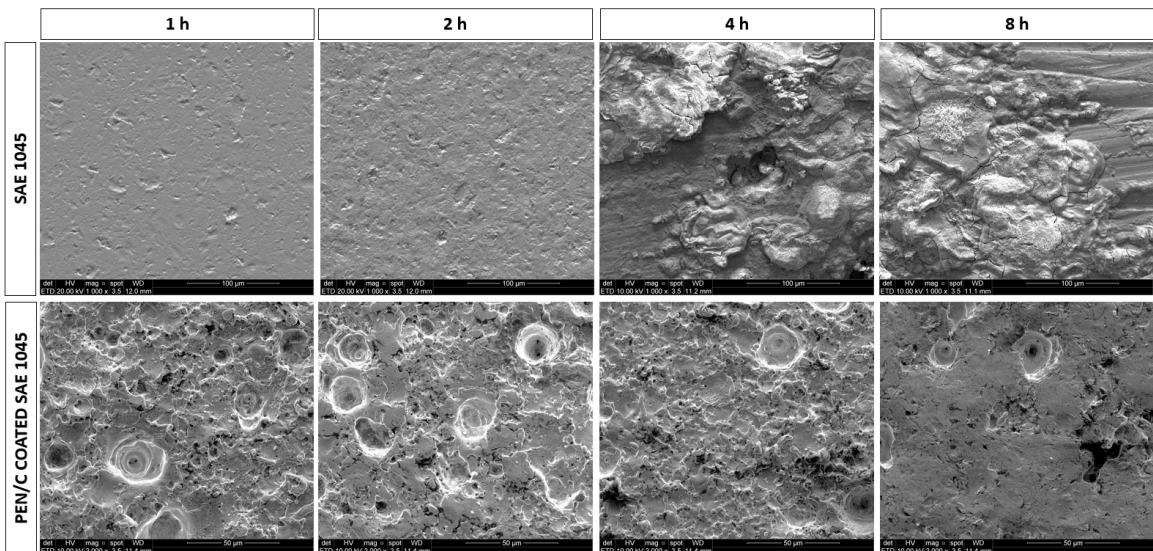


**Figure 7.** SEM of SAE 1045 and PEN/C coated SAE 1045 samples after ESEWT tests/ polarization curve.

In the case of PEN/C coated SAE 1045, as it is a material to replace with a fragile coating, the mechanisms involved were different. As shown in Figure 7, increasing the test time removed the characteristic surface irregularities of the coating (Figure 1), leading to a decrease in the surface roughness of the coatings (Figure 8). This behaviour was more pronounced at 8 h of testing. The wear resistance of this coating prevented the formation of surface cracks, even in the longest test. In addition, the coating remained intact in all conditions tested, due to the low rates of mass loss by erosion and corrosion. It is noted that even after 8 hours of testing, the characteristic topography of the PEN/C coating (basically the pores and discharge channels) is still observed on the surface, showing that the coating is present.

### 3.2.3. Determination of synergism between wear and corrosion

To determine the synergism between the tribological and corrosive phenomena that acted during the ESEWT test, the recommendations of ASTM G119[22] were used. The components related to erosive wear, corrosion and the synergy between the phenomena are shown in Figure 9.

Analysing the phenomena involved in SAE 1045 steel (Figure 9A), the synergy between erosion and corrosion was the predominant factor in the mass loss of these samples. Possibly, the removal of the corrosion product during the test, as well as the decrease in corrosion resistance generated by the surface hardening of these samples, potentiated the mass loss of the uncoated substrate. In addition, despite the decrease in the wear rate in the longer tests, the synergy factor is responsible for approximately 85 % of the material loss of the SAE 1045 steel in the ESEWT test (Figure 9C). Due to surface hardening, the participation of erosive wear decreased in the mass loss rate, being responsible for approximately 12 % in the 1 h test, reducing to 7.5 % in the 8 h test. This phenomenon led to a decrease in corrosion resistance and an increase in the participation of this event, which were approximately 2.7 % in the 1 h test and 8.6% in the 8 h test. It is noteworthy that erosive wear occurs even with eroded particles smaller than 100 μm (Figure 3A).
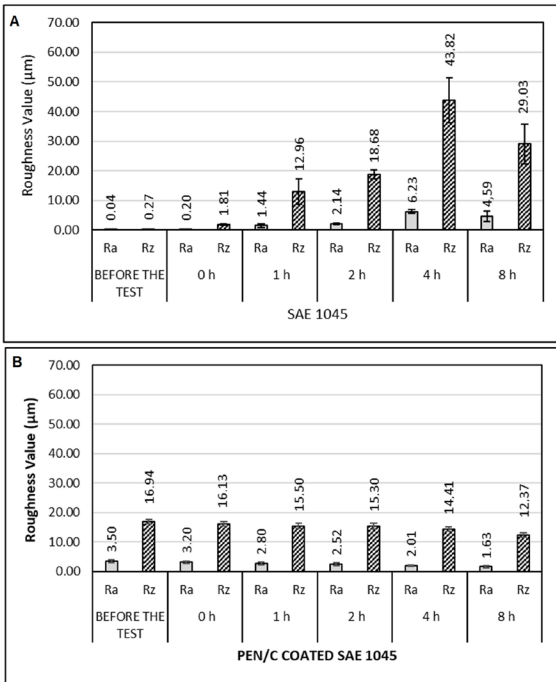


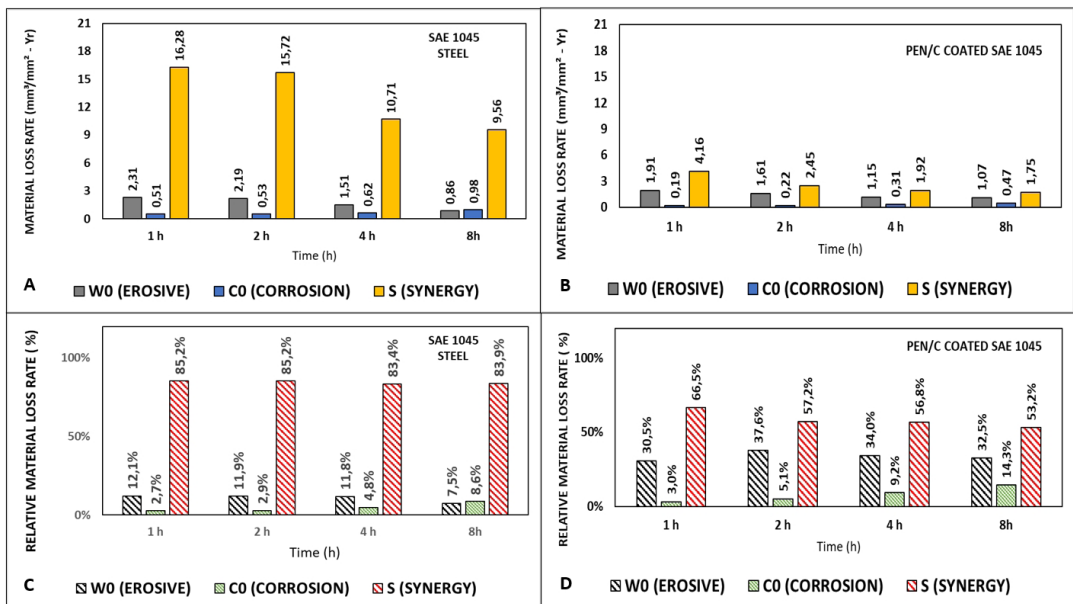**Figure 8.** Surface roughness after ESEWT tests.



**Figure 9.** Mass loss rate and percentage of the relative material loss rate of factors that separately influence the process as a function of exposure time. A: SAE 1045 steel; B: PEN/C coated SAE 1045; C: Percentage of SAE 1045 steel; D: Percentage of PEN/C coated SAE 1045.

Tests on samples with PEN/C coated SAE 1045 (Figure 9B and Figure 9D) demonstrated the ability to reduce the synergy, erosive wear, and corrosion of the metallic substrate. Synergy was also the main component responsible for the mass loss rate of these samples, although, as previously demonstrated, at values substantially lower than those of the uncoated substrate. The erosion component did not show a clear behaviour trend, varying between approximately 30 % and 37 % of the material loss rate (Figure 9D). Another important point is related to the increase in the corrosion component in the mass loss of the samples with the nitrocarburized layer (Figure 9D). As previously mentioned, corrosion in these samples predominantly occurred in the pores formed by the discharge channels (Figure 4B and Figure 4C). Within the pores, a process of local modification of the electrolyte must occur over time, as it becomes occluded in these places, reducing the pH and increasing the concentration of chlorides in relation to the bulk of the solution[50]. This localized reduction in pH, due to the increased presence of H+, naturally attracts the migration of Cl- ions, increasing corrosivity within the pores. Furthermore, it is possible that the erosive effect and the possible reduction in corrosion resistance, as the test time increased, may have contributed to the increased participation of corrosion in the rate of mass loss.

### 3.2.4. Effect of ESEWT test time

To determine how the erosive wear affects the corrosion resistance over time, ESEWT tests were performed at different times (zero, 1 h, 2 h, 4 h, 8 h), all under cathodic protection, thus, there was no participation of corrosion in the process degradation, just wear. After each time, polarization curves were performed. The objective of this procedure is to evaluate how the wear generated by the slurry on the sample surface would change the corrosion resistance of the two types of samples studied: substrate (SAE 1045) and the substrate with the PEN/C layer. Therefore, the purpose of this test would be to evaluate the role of wear in reducing the rate of mass loss over time, observed in the substrate and in the PEN/C layer, as shown in item 3.2.2 and Figure 6. Therefore, no considerable corrosive effects occurred during

the test time before the polarization curve, only erosion wear. The results are shown in Figure 10 and Table 3. Note that increasing the time of the experiment, before carrying out the polarization curves, in the tests for SAE 1045 steel without coating (Figure 10A) led to a gradual decrease in Ecorr and an elevation of Icorr, indicating an increase in susceptibility to corrosion of the SAE 1045 steel clearly due to the erosive action of the medium (particles + fluid). This generated an increase in the surface roughness of the substrate (Figure 7 and Figure 8) and the consequent surface hardening mentioned previously[45]. It has been known since the 1960s that plastic deformations increase the corrosion rate of steels[51]. Oluwaseun and Simeon[52] demonstrated the effect of plastic deformation on the increase in the corrosion rate of a medium-carbon steel alloy in an environment containing NaCl. Thus, the surface plastic deformation induced by the impact of the silica particles, driven by the speed of the fluid moving on the surface of the samples, increased the corrosivity of the SAE 1045 steel samples, leading to a CR of 0.98 mm.year $^{-1}$ after 8 h of ESEWT test. That way, the most aggressive condition for the uncoated samples was after 8 hours of testing, with an $E_{corr}$ of - 472 mV$_{sce}$ and an $I_{corr}$ of 7.7 x 10$^{-5}$ A.cm$^{-2}$ (obtained by Tafel extrapolation method).

In the case of PEN/C coated SAE 1045 samples, increasing the test time, before carrying out the polarization curves in the coated tests did not significantly influence the behaviour of the polarization curves (Figure 10B and Table 3). Observing the values relating to the corrosion potential and the corrosion currents obtained by the Tafel extrapolation method, it can be seen that the values are in the same order of magnitude, without showing a tendency for increase or reduction. This demonstrated that the coatings maintained their protective capacity, even after 8 hours of erosion testing. Thus, as the values of $E_{corr}$ and $I_{corr}$ showed very similar values, leading to significantly lower CR than the uncoated tests (Table 3). Therefore, the increase in the corrosion component in the uncoated SAE 1045 steels (Figure 9C) is due to the increase in the surface corrosivity of the substrate, while in the nitrocarburized samples the layer maintained its protective capacity, even after 8 hours of testing.
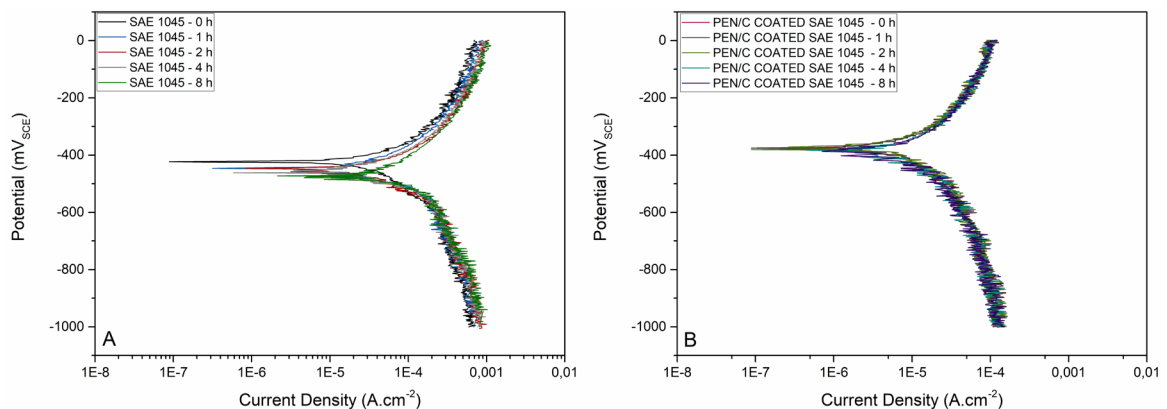


**Figure 10.** Polarization curves after increasing exposure times (time exposure) in cathodic protection. A: SAE 1045 steel; B: PEN/C coated SAE 1045.

**Table 3.** $E_{corr}$ and $I_{corr}$ values in the after-time exposure in cathodic protection.

| Sample | Parameter | Cathodic protection test time | | | | |
|---|---|---|---|---|---|---|
| | | zero | 1 h | 2 h | 4 h | 8 h |
| SAE 1045 | $\dfrac{E_{corr}}{(mV_{sce})}$ | - 423 | - 446 | - 447 | - 461 | - 472 |
| | $\dfrac{I_{corr}}{[10^{-5}]}$ $(A.cm^{-2})$ | 2.31 | 3.00 | 3.30 | 4.60 | 7.70 |
| | $\dfrac{CR}{(mm.y^{-1})}$ | 0.35 | 0.51 | 0.53 | 0.62 | 0.98 |
| PEN/C COATED SAE 1045 | $\dfrac{E_{corr}}{(mV_{sce})}$ | - 375 | - 378 | - 380 | - 383 | - 387 |
| | $\dfrac{I_{corr}}{[10^{-5}]}$ $(A.cm^{-2})$ | 0.61 | 0.62 | 0.64 | 0.70 | 0.75 |
| | $\dfrac{CR}{(mm.y^{-1})}$ | 0.13 | 0.19 | 0.22 | 0.31 | 0.47 |

This test showed that the erosion suffered on the surface, over the test time, did not increase the susceptibility to corrosion of the PEN/C layer, probably because there was no significant hardening, due to the superior hardness of the layer in relation to the substrate. Furthermore, despite the high hardness of the PEN/C layer, indicating fragility, no peeling of that layer was detected. Therefore, the increase in the corrosion component detected for these samples (Figure 9D) and discussed in item 3.2.3 is due to variations in the occluded electrolyte inside the coating pores, leading to increased corrosion rate with time.

## 4. Conclusions

The main conclusions, based on the results of the ESEWT tests, are presented below:
- The PEN/C coated SAE 1045 showed superior resistance to erosive wear and corrosion than the uncoated SAE 1045 steel. However, the pores formed by the discharge channels during the coating formation process favoured the occurrence of localized corrosion inside the pores, due to the changes that occurred in the occluded electrolyte in these cavities.
- The study, carried out according to the ASTM G119 standard, demonstrated that the synergy was the main factor in the mass loss rates of the SAE 1045 steel and of the samples with PEN/C coated SAE 1045.
- The synergistic mechanism of the uncoated sample occurred by removing the corrosion product formed, which could act as a kind of barrier, and by activating the surface given by the plastic deformation generated by the erosive process of the particles.
- The synergistic mechanism of PEN/C coated SAE 1045 occurred with the removal of surface irregularities, inherent to this layer, by the erosive process, combined with localized corrosion within the pores.

- Tests with cathodic protection, followed by polarization curves, showed how and if wear acts on the corrosive process over time. In the case of SAE 1045, surface tensions and deformations were increased, which intensified dissolution by corrosion. In the case of PEN/C coated SAE 1045, due to the high hardness of the coating, this factor hardly interferes. In this test, corrosion increases over time, as localized corrosion occurs in the coating pores, which tend to increase their aggressiveness over time.

## 6. References

1. Belkin PN, Naumov A, Shadrin S, Dyakov IG, Zhirov A, Kusmanov SA, et al. Anodic plasma electrolytic saturation of steels by carbon and nitrogen. Adv Mat Res. 2013;704:37-42. http://dx.doi.org/10.4028/www.scientific.net/AMR.704.37.
2. Kusmanov SA, Grishina EP, Belkin PN, Kusmanova YV, Kudryakova NO. Raising the corrosion resistance of low-carbon steels by electrolytic-plasma saturation with nitrogen and carbon. Metal Sci Heat Treat. 2017;59(1-2):117-23. http://dx.doi.org/10.1007/s11041-017-0114-0.
3. Belkin PN, Yerokhin A, Kusmanov SA. Plasma electrolytic saturation of steels with nitrogen and carbon. Surf Coat Tech. 2016;307:1194-218. http://dx.doi.org/10.1016/j.surfcoat.2016.06.027.
4. Lin N, Xie R, Zhou P, Zou J, Ma Y, Wang Z, et al. Review on improving wear and corrosion resistance of steels via plasma electrolytic saturation technology. Surf Rev Lett. 2016;23(4):1630002. http://dx.doi.org/10.1142/S0218625X16300021.

5.  Noori SM, Dehghanian C. Characterization of nitrocarburized coating by plasma electrolytic saturation. Acta Metall Slovaca. 2018;24(1):20. http://dx.doi.org/10.12776/ams.v24i1.957.

6.  Benlahreche FZ, Nouicer E. Improvement of surface properties of low carbon steel by nitriding treatment. Acta Phys Pol A. 2017;131(1):20-3. http://dx.doi.org/10.12693/APhysPolA.131.20.

7.  Padervand S, Amiri M, Mousavi khoei M. Optimization of electrolyte concentration for surface modification of tantalum using plasma electrolytic nitridation. Int J Refract Hard Met. 2020;87:105146. http://dx.doi.org/10.1016/j.ijrmhm.2019.105146.

8.  Tambovskiy I, Mukhacheva T, Gorokhov I, Suminov I, Silkin S, Dyakov I, et al. Features of cathodic plasma electrolytic nitrocarburizing of low-carbon steel in an aqueous electrolyte of ammonium nitrate and glycerin. Metals (Basel). 2022;12(10):1773. http://dx.doi.org/10.3390/met12101773.

9.  Yerokhin AL, Nie X, Leyland A, Matthews A, Dowey SJ. Plasma electrolysis for surface engineering. Surf Coat Tech. 1999;122(2-3):73-93. http://dx.doi.org/10.1016/S0257-8972(99)00441-7.

10.  Rocha JL, Pereira RS, de Oliveira MCL, Antunes RA. Investigation on the relationship between the surface chemistry and the corrosion resistance of electrochemically nitrided AISI 304 stainless steel. International Journal of Corrosion. 2019;7023283. https://doi.org/10.1155/2019/7023283.

11.  Desale GR, Gandhi BK, Jain SC. Effect of physical properties of solid particle on erosion wear of ductile materials. USA: American Society of Mechanical Engineers Digital Collection; 2008.

12.  Noon AA, Kim M-H. Erosion wear on centrifugal pump casing due to slurry flow. Wear. 2016;364–365:103-11. http://dx.doi.org/10.1016/j.wear.2016.07.005.

13.  Wood RJK. Erosion–corrosion interactions and their effect on marine and offshore materials. Wear. 2006;261(9):1012-23. http://dx.doi.org/10.1016/j.wear.2006.03.033.

14.  Yao Z, Zheng Y, Ke W. The influence of applied potential on the erosion-corrosion behavior of AISI321 stainless steel in acidic slurry medium. Wear. 1995;186–187:568-72. http://dx.doi.org/10.1016/0043-1648(95)07134-2.

15.  Ludwig GA, Malfatti CF, Schroeder RM, Ferrari VZ, Muller IL. WC10Co4Cr coatings deposited by HVOF on martensitic stainless steel for use in hydraulic turbines: resistance to corrosion and slurry erosion. Surf Coat Tech. 2019;377:124918. http://dx.doi.org/10.1016/j.surfcoat.2019.124918.

16.  Goyal K. Mechanical properties and erosive behaviour of 10TiO2-Cr2O3 coated CA6NM turbine steel under accelerated conditions. World J Eng. 2019;16(1):64-70. http://dx.doi.org/10.1108/WJE-08-2018-0262.

17.  Kumar R, Goyal K, Bhandari D. Slurry erosion behavior of thermally sprayed ceramic nanocomposite coatings on turbine steel. Int J Appl Ceram Technol. 2022;19(6):3049-61. http://dx.doi.org/10.1111/ijac.14117.

18.  Nguyen QB, Lim CYH, Nguyen VB, Wan YM, Nai B, Zhang YW, et al. Slurry erosion characteristics and erosion mechanisms of stainless steel. Tribol Int. 2014;79:1-7. http://dx.doi.org/10.1016/j.triboint.2014.05.014.

19.  Javaheri V, Haiko O, Sadeghpour S, Valtonen K, Kömi J, Porter D. On the role of grain size on slurry erosion behavior of a novel medium-carbon, low-alloy pipeline steel after induction hardening. Wear. 2021;476:203678. http://dx.doi.org/10.1016/j.wear.2021.203678.

20.  Desale GR, Gandhi BK, Jain SC. Slurry erosion of ductile materials under normal impact condition. Wear. 2008;264(3-4):322-30. http://dx.doi.org/10.1016/j.wear.2007.03.022.

21.  Câmara Noronha L, Velho de Castro V, Ludwig GA, Moreira Schroeder R, de Fraga Malfatti C. Ti–Cp: eletrochemical behaviour under slurry erosion wear. J Bio Tribocorros. 2020;7(1):8. http://dx.doi.org/10.1007/s40735-020-00442-y.

22.  ASTM: American Society for Testing and Materials. ASTM G119-09(2016) - Standard Guide for Determining Synergism Between Wear and Corrosion. West Conshohocken: ASTM; 2016 [cited 2022 Oct 19]. Available from: https://webstore.ansi.com/Standards/ASTM/ASTMG119092016?gclid=CjwKCAjwwL6aBhBlEiwADycBIDBOao12w6R67kDR4USNK7Z12OuUeOnXFcHnFKv_nD98okxCYvdZNBoCb7kQAvD_BwE

23.  Sun B, Fan J, Wen D, Chen Y. An experimental study of slurry erosion involving tensile stress for pressure pipe manifold. Tribol Int. 2015;82:280-6. http://dx.doi.org/10.1016/j.triboint.2014.07.025.

24.  ASTM International. ASTM G102-89 Standard Practice for Calculation of Corrosion Rates and Related Information from Electrochemical Measurements. West Conshohocken: ASTM International; 1994 [cited 2021 Nov 8]. Available from: https://www.astm.org/Standards/G102.

25.  ISO: International Organization for Standardization. ISO 4287:1997 Geometrical Product Specifications (GPS) — Surface texture: Profile method — Terms, definitions and surface texture parameters. Geneva: ISO; 1997.

26.  Wu J, Xue W, Wang B, Jin X, Du J, Li Y. Characterization of carburized layer on T8 steel fabricated by cathodic plasma electrolysis. Surf Coat Tech. 2014;245:9-15. http://dx.doi.org/10.1016/j.surfcoat.2014.02.024.

27.  Wu J, Wang K, Fan L, Dong L, Deng J, Li D, et al. Investigation of anodic plasma electrolytic carbonitriding on medium carbon steel. Surf Coat Tech. 2017;313:288-93. http://dx.doi.org/10.1016/j.surfcoat.2017.01.109.

28.  Hua X-Z, Zhou L, Cui X, Zou A-H, Xu W-B, Zhou X-L. The Effect of Ammonia Water on the Microstructure and Performance of Plasma Electrolytic Saturation Nitriding Layer of 38CrMoAl Steel. Phys Procedia. 2013;50:304-14. http://dx.doi.org/10.1016/j.phpro.2013.11.049.

29.  Kusmanov SA, Silkin SA, Smirnov AA, Belkin PN. Possibilities of increasing wear resistance of steel surface by plasma electrolytic treatment. Wear. 2017;386–387:239-46. http://dx.doi.org/10.1016/j.wear.2016.12.053.

30.  Shen D-J, Wang Y-L, Nash P, Xing G-Z. A novel method of surface modification for steel by plasma electrolysis carbonitriding. Mater Sci Eng A. 2007;458(1-2):240-3. http://dx.doi.org/10.1016/j.msea.2006.12.067.

31.  Dalcin RL, Rocha AS, Castro VV, Oliveira LF, Neves JCK, Silva CH, et al. (2021) Influence of plasma nitriding with a nitrogen rich gas composition on the reciprocating sliding wear of a DIN 18MnCrSiMo6-4 steel. Mat Res. 24(4):e20200592. https://doi.org/10.1590/1980-5373-MR-2020-0592.

32.  Dalcin RL, Rocha A S, Castro VV, Neves JCK, Silva CH, Torres RD, et al. Microstructure and wear properties of a low carbon bainitic steel on plasma nitriding at different $N_2$-$H_2$ gas mixtures. Mat Res. 2021;25:e20210447. https://doi.org/10.1590/1980-5373-MR-2021-0447.

33.  Karakan M, Alsaran A, Çelik A. Effect of process time on structural and tribological properties of ferritic plasma nitrocarburized AISI 4140 steel. Mater Des. 2004;25(4):349-53. http://dx.doi.org/10.1016/j.matdes.2003.10.017.

34.  Çelik A, Karakan M, Alsaran A, Efeoglu I. The investigation of structural, mechanical and tribological properties of plasma nitrocarburized AISI 1020 steel. Surf Coat Tech. 2005;200(5-6):1926-32. http://dx.doi.org/10.1016/j.surfcoat.2005.08.027.

35.  Li Y, Ye Q, Zhu Y, Zhang L, He Y, Zhang S, et al. Microstructure, adhesion and tribological properties of CrN/CrTiAlSiN/WCrTiAlN multilayer coatings deposited on nitrocarburized AISI 4140 steel. Surf Coat Tech. 2019;362:27-34. http://dx.doi.org/10.1016/j.surfcoat.2019.01.091.

36.  Liebhard M, Levy A. The effect of erodent particle characteristics on the erosion of metals. Wear. 1991;151(2):381-90. http://dx.doi.org/10.1016/0043-1648(91)90263-T.

37. Clark HM, Llewellyn RJ. Assessment of the erosion resistance of steels used for slurry handling and transport in mineral processing applications. Wear. 2001;250(1-12):32-44. http://dx.doi.org/10.1016/S0043-1648(01)00628-7.

38. Lynn RS, Wong KK, Clark HMI. On the particle size effect in slurry erosion. Wear. 1991;149(1-2):55-71. http://dx.doi.org/10.1016/0043-1648(91)90364-Z.

39. Gandhi BK, Borse SV. Nominal particle size of multi-sized particulate slurries for evaluation of erosion wear and effect of fine particles. Wear. 2004;257(1-2):73-9. http://dx.doi.org/10.1016/j.wear.2003.10.013.

40. Clark HMI, Hartwich RB. A re-examination of the 'particle size effect' in slurry erosion. Wear. 2001;248(1-2):147-61. http://dx.doi.org/10.1016/S0043-1648(00)00556-1.

41. Nie X, Wang L, Yao ZC, Zhang L, Cheng F. Sliding wear behaviour of electrolytic plasma nitrided cast iron and steel. Surf Coat Tech. 2005;200(5-6):1745-50. http://dx.doi.org/10.1016/j.surfcoat.2005.08.046.

42. Revenko VG, Parshutin VV, Chernova GP, et al. Effect of nitriding during electrolytic heating on the electrochemical and corrosion behavior of ST45. Elektronnaya Obrabotka Materialov. 1985;56-9.

43. Kalendová A, Veselý D, Kalenda P. Properties of paints with hematite coated muscovite and talc particles. Appl Clay Sci. 2010;48(4):581-8. http://dx.doi.org/10.1016/j.clay.2010.03.007.

44. Belkin PN, Dyakov IG, Zhirov AV, Kusmanov SA, Mukhacheva TL. Effect of compositions of active electrolytes on properties of anodic carburization. Prot Met Phys Chem Surf. 2010;46(6):715-20. http://dx.doi.org/10.1134/S2070205110060158.

45. Wang Q, Wang J. Investigation of wear property and strengthening mechanism of hot-rolled medium manganese steel on condition of slurry erosion wear. J Tribol. 2022;145(1):011703. http://dx.doi.org/10.1115/1.4055716.

46. Heinz K, Gahr Z. Microstructure and wear of materials. New York: Elsevier; 1987.

47. Finnie I. Erosion of surfaces by solid particles. Wear. 1960;3(2):87-103. http://dx.doi.org/10.1016/0043-1648(60)90055-7.

48. Javaheri V, Porter D, Kuokkala V-T. Slurry erosion of steel – review of tests, mechanisms and materials. Wear. 2018;408-409:248-73. http://dx.doi.org/10.1016/j.wear.2018.05.010.

49. Clark HMI, Wong KK. Impact angle, particle energy and mass loss in erosion by dilute slurries. Wear. 1995;186-187:454-64. http://dx.doi.org/10.1016/0043-1648(95)07120-2.

50. Cramer SD, Covino BS. Pitting corrosion. In: Cramer SD, Covino BS Jr, editors. Corrosion: fundamentals, testing, and protection. West Conshohocken: ASM International; 2003. p. 236-41. http://dx.doi.org/10.31399/asm.hb.v13a.a0003612.

51. Greene ND, Saltzman GA. Effect of plastic deformation on the corrosion of iron and steel. Corrosion. 2013;20(9):293t-8t. http://dx.doi.org/10.5006/0010-9312-20.9.293t.

52. Alo OA, Ibitoye SA. Effect of induced stress on the corrosion rate of medium carbon steel in saline environment. J Chem Eng Mater Sci. 2015;6(4):52-9. http://dx.doi.org/10.5897/JCEMS2015.0221.